

# Does carrier localization affect the anomalous Hall effect?

Prasanta Chowdhury<sup>1</sup>, Mohamad Numan<sup>1</sup>, Shuvankar Gupta<sup>2</sup>,  
Souvik Chatterjee<sup>3</sup>, Saurav Giri<sup>1</sup>, Subham Majumdar<sup>1\*</sup>

<sup>1</sup>*School of Physical Sciences, Indian Association for the Cultivation of Science,  
2A & B Raja S. C. Mullick Road, Jadavpur, Kolkata 700 032, India*

<sup>2</sup>*Condensed Matter Physics Division, Saha Institute of Nuclear Physics,  
1/AF, Bidhannagar, Kolkata, 700 064, India and*

<sup>3</sup>*UGC-DAE Consortium for Scientific Research, Kolkata Centre,  
Sector III, LB-8, Salt Lake, Kolkata 700106, India*

The effect of carrier localization due to electron-electron interaction in anomalous Hall effect is elusive and there are contradictory results in the literature. To address the issue, we report here the detailed transport study including the Hall measurements on  $\beta$ -Mn type cubic compound  $\text{Co}_7\text{Zn}_7\text{Mn}_6$  with chiral crystal structure, which lacks global mirror symmetry. The alloy orders magnetically below  $T_c = 204$  K, and reported to show spin glass state at low temperature. The longitudinal resistivity ( $\rho_{xx}$ ) shows a pronounced upturn below  $T_{min} = 75$  K, which is found to be associated with carrier localization due to quantum interference effect. The upturn in  $\rho_{xx}$  shows a  $T^{1/2}$  dependence and it is practically insensitive to the externally applied magnetic field, which indicate that electron-electron interaction is primarily responsible for the low- $T$  upturn. The studied sample shows considerable value of anomalous Hall effect below  $T_c$ . We found that the localization effect is present in the ordinary Hall coefficient ( $R_0$ ), but we failed to observe any signature of localization in the anomalous Hall resistivity or conductivity. The absence of localization effect in the anomalous Hall effect in  $\text{Co}_7\text{Zn}_7\text{Mn}_6$  may be due to large carrier density, and it warrants further theoretical investigations, particularly with systems having broken mirror symmetry.

## I. INTRODUCTION

The ordinary Hall (OH) effect, which arises from the deflection of the moving charge carriers due to Lorentz force, was discovered in 1879 [1], and its underlying mechanism is in general considered to be well comprehended. In contrast, the anomalous Hall effect (AHE) [2, 3] observed in magnetic materials has remained relatively subtle. The phenomenon is intriguing both from fundamental point of view as well as for its potential applications in sensors, memories and logics [4, 5]. It is now well recognized that there are mainly three mechanisms responsible for AHE, namely, intrinsic mechanism, skew scattering and side-jump [5]. Karplus and Luttinger were first to suggest that intrinsic mechanism arises from transverse velocity of the Bloch electrons induced by spin-orbit interaction (SOI) and interband mixing [6], and recently Xiao *et al.* reinterpreted it in terms of Berry curvature of the occupied Bloch states [7]. The other two mechanisms (skew scattering and side-jump) are extrinsic in nature and they arise from the asymmetric scattering of the conduction electrons by the impurities in presence of SOI as proposed by Smit [8, 9] and Berger [10]. Depending upon its origin, the anomalous Hall resistivity ( $\rho_{xy}^{AHE}$ ) scales differently with longitudinal resistivity ( $\rho_{xx}$ ). The skew scattering is generally observed in highly conducting metals ( $\rho_{xx} \lesssim 10^{-6} \Omega \text{ cm}$ ) with low amount of impurities [5] and it varies as  $\rho_{xy}^{AHE} \propto \rho_{xx}$ . On the other hand, both intrinsic and side-jump mechanisms follow  $\rho_{xy}^{AHE} \propto \rho_{xx}^2$ .

However, the situation is far more complex, if a comparatively higher degree of disorder is present in the magnetic metal ( $\rho_{xx} \gtrsim 10^{-3} \Omega \text{ cm}$ ). In presence of disorder, the quantum effects become more prominent, and the system can show localization of charge carriers due to electron-electron coulomb interaction (EEI), disordered induced weak localization (WL), or Kondo effect [5, 11, 12]. As a result, metallic  $\rho_{xx}(T)$  exhibits an upturn ( $d\rho_{xx}(T)/dT < 0$ ) at low temperature ( $T$ ), and a resistivity minimum (at  $T_{min}$ ) is observed [12–16]. The effect of quantum corrections has been extensively studied for longitudinal conductivity and conventional Hall effect [11, 12, 17], but it is still poorly understood in case of AHE.

There are few recent theoretical and experimental works addressing the effect of localization on AHE [14, 16, 18–27]. It is shown theoretically that WL does not contribute towards side-jump mechanism, but it can have nonzero contribution in skew scattering [18, 19]. On the other hand, EEI correction to AHE identically vanishes for both skew scattering and side-jump due to general symmetry reasons [19, 20]. The above theoretical prediction of the absence of EEI correction towards AHE was experimentally verified in  $\text{Co}_2\text{FeSi}$  Heusler alloy thin film [13] and  $\text{Zr}_{1-x}\text{V}_x\text{Co}_{1.6}\text{Sn}$  semimetal [27]. On the other hand, WL correction was experimentally observed in polycrystalline Fe, Ni, FePt and amorphous CoFeB films [14, 21–24]. However, there are some disordered systems, which do not follow the above rules. For example, WL effect in AHE is found to be absent in the disordered ferromagnets  $\text{Ga}_{1-x}\text{Mn}_x\text{As}$  [16]. Similarly, a pronounced low- $T$  EEI correction to AHE was observed in the magnetic semiconductor  $\text{HgCr}_2\text{Se}_4$  [25].

\* [sspsm2@iacs.res.in](mailto:sspsm2@iacs.res.in)

A recent theoretical work proposed that the low- $T$  EEI correction could exist and anomalous Hall conductivity (AHC) should follow as  $T^{1/2}/\ln(T_0/T)$  in three dimensional (3D) [26] material. Therefore, the effect of disorder on AHE remains inconclusive both theoretically and experimentally.

In the previous experimental works addressing the localization effect on AHE, the majority of the works are on systems having WL. There are only few experimental reports where EEI is the primary cause of the localization [13, 25, 27]. However, those few systems where EEI is prevalent, the temperature window where the upturn in  $\rho_{xx}(T)$  is observed (*i.e.*, the region where EEI mediated localization dominates) is narrow ( $T_{min}$  is 30 K or less), and the upturn is rather weak. To examine the role of EEI in AHE, it is important to search for a system showing significant upturn in  $\rho_{xx}(T)$  over a large  $T$  range. For the present study, we chose  $\beta$ -Mn-type  $\text{Co}_7\text{Zn}_7\text{Mn}_6$  alloy, which can be thought of being derived from  $\text{Co}_{10}\text{Zn}_{10}$  by the substitution of Co and Zn by Mn. Below a critical temperature  $T_c \sim 480$  K,  $\text{Co}_{10}\text{Zn}_{10}$  undergoes a transition from paramagnetic state to helimagnetic state [28, 29] and  $T_c$  decreases with the partial substitution of Mn. Just below  $T_c$ , it exhibits skyrmionic state in a small  $T$  and field ( $H$ ) ( $100 \text{ Oe} \lesssim H \lesssim 400 \text{ Oe}$ ) windows. At higher  $H$  ( $H > 1 \text{ kOe}$ ), the sample attains a completely ferromagnetic (FM) state. This alloy has a chiral cubic crystal structure (enantiomeric space group:  $P4_132$  or  $P4_332$ , depending on its handedness) and the unit cell contains 20 atoms which are distributed over two Wyckoff sites [8c and 12d, see Fig. 1 (a)] [29, 30]. Previous studies reveal that 8c sites are mainly occupied by Co atoms while Zn and Mn atoms prefer the hyper kagomé network of 12d sites [31–33]. Due to multiple crystallographic sites and similar radii of Mn, Co and Zn atoms, antisite disorder is very likely to occur in these  $\beta$ -Mn-type alloys [32, 33]. These materials are ideal test beds for studying the disorder effect in AHE, because they show, (i) long range magnetic ordering with spontaneous magnetization, and have (ii) chiral structure lacking both inversion and mirror symmetry, which can lead to intrinsic Berry phase induced Hall effect.

Till now Co-Zn-Mn alloys mostly studied to explore the skyrmionic state [29, 34, 35] via magnetization, ac susceptibility, small angle neutron scattering and transmission electron microscopy. However, little attention is given to their electronic transport properties. In fact previous Hall studies on Co-Zn-Mn gave some contradictory results. Zeng *et al.* reported the main mechanism behind the AHE to be skew scattering [37], while Qi *et al.* found the dominance of intrinsic mechanism [36]. In the present work, we have carefully investigated the AHE in the alloy  $\text{Co}_7\text{Zn}_7\text{Mn}_6$  with the intention to see whether the effect of carrier localization is affecting it. Our work indicates that the sample shows upturn in  $\rho_{xx}$  due to EEI, while AHE remains unaffected, which substantiates the theory proposed by Muttalib and Wölfle, and Langenfeld and Wölfle [19, 20].

## II. EXPERIMENTAL DETAILS

A polycrystalline sample of  $\text{Co}_7\text{Zn}_7\text{Mn}_6$  was synthesized by the method as described in previous report by Kosuke Karubel *et al.* [34]. The structural investigation of the sample was performed by powder x-ray diffraction (PXRD) in the  $T$  range 10–300 K, using RIGAKU Smartlab (9KW) XG diffractometer fitted with a helium closed cycle refrigerator, using  $\text{Cu K}\alpha$  radiation. The Rietveld refinement of the XRD data was performed using the MAUD software package [38]. Magnetic measurements were carried out using the vibrating sample magnetometer module of a commercial physical properties measurement system (PPMS, Quantum Design) as well as on a SQUID-VSM (MPMS3) of Quantum Design. The standard four-probe technique was used to measure  $\rho_{xx}$  on a cryogen-free high magnetic field system (Cryogenic Ltd. UK) between 5 and 300 K. Hall measurements were performed using Physical Properties Measurement System (Quantum design Inc., USA) using four probe technique.

## III. RESULTS

### A. Powder X-ray diffraction

The Rietveld refinement of the temperature dependent PXRD data indicate that the sample retains its cubic structure with space group  $P4_132$ , down to the lowest measured temperature of 10 K [Fig. 1 (b)]. Fig. 1 (c) shows the thermal variation of lattice parameter  $a$  (in Å). The cubic lattice parameter  $a$  decreases monotonically down to 40 K with lowering of  $T$ . Interestingly, below 40 K, we notice a clear anomaly as  $a$  increases with decreasing  $T$ . As a result, we find a minimum at around 40 K in the  $a$  versus  $T$  data, and the data below 40 K show a negative thermal expansion ( $da/dT < 0$ ).

### B. Magnetization

Fig. 2 (a) shows the  $T$  variation of magnetization ( $M$ ) in an externally applied magnetic field of  $H = 100 \text{ Oe}$ . The measurements were performed in zero-field-cooled-heating (ZFC), field-cooling (FC) and field-cooled-heating (FCH) protocols. The  $T$ -dependence of  $dM/dT$  for FC and FCH measurements is shown in the inset of Fig. 2 (a). From the minimum of the  $dM/dT$  vs  $T$  plot, the transition from paramagnetic state to a helimagnetic state [28, 29, 39] is found to be at  $T_c \sim 204$  K. Interestingly, around  $T_c$ , there is a clear thermal hysteresis between FC and FCH data which indicates a first order like magnetic transition. The hysteresis is present for different temperature ramping rates (5 K and 10 K per min) and also for different magnetometers (PPMS and SQUID-VSM). However,  $T$  dependent PXRD does not show any major anomaly in  $a$  around  $T_c$  [see Fig. 1 (c)], and it rules out any structural change at  $T_c$ . A sharp

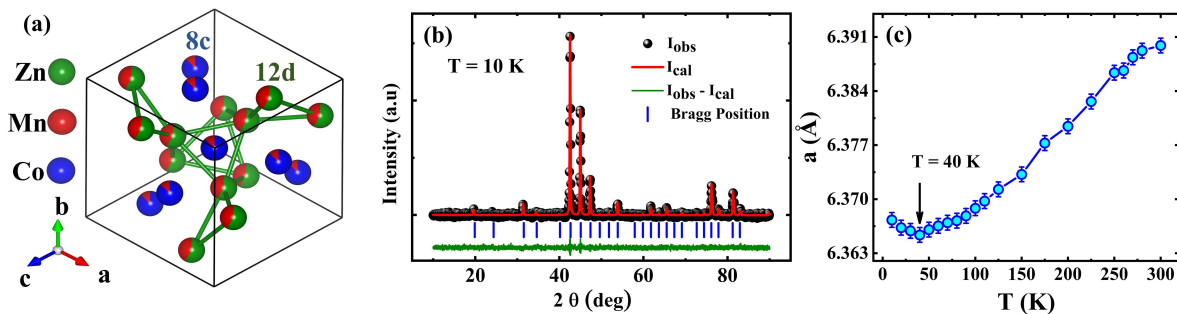


FIG. 1. (a) Crystal structure of  $\text{Co}_7\text{Zn}_7\text{Mn}_6$  ( $P4_132$ -right handed structure) as viewed along the  $[111]$  direction. (b) Powder x-ray diffraction pattern of  $\text{Co}_7\text{Zn}_7\text{Mn}_6$  (data points) and Rietveld refinement curves (solid line) at 10 K and (c) Depict the thermal variation of lattice parameter( $a$ )

drop of  $M$  below 35 K is observed in the ZFC data, which matches well with the onset of reentrant spinglass state reported previously based on ac susceptibility measurements [32, 33]. The spin glass transition is likely due to the geometrical frustration, which is intrinsic to  $\beta$ -Mn type structure, and disorder present in the system [34]. Our  $T$  dependent PXRD [see Fig. 1 (c)] result shows an anomaly in lattice parameter at below 40 K, which is close to the spin-glass freezing temperature. This may indicate a close interplay between magnetic and structural aspects in the sample.

We have examined the  $\chi^{-1}$  vs  $T$  data measured at  $H = 1$  kOe between 220 to 315 K, and it is shown in the right panel of Fig. 2 (b).  $\chi^{-1}$  is seen to deviate from linearity below 285 K and from linear fit above 285 K, we obtain Weiss temperature ( $\theta_p$ ) to be 238 K, which is quite high as compared to  $T_c$ . We also tried to fit the  $\chi$  vs  $T$  data with modified Curie-Weiss law:  $\chi = \chi_0 + C/(T - \theta_p)$ , where  $\chi_0$  is a  $T$  independent term,  $C$  is the Curie constant and  $\theta_p$  is the Weiss temperature. As we can see from the left panel of Fig. 2 (b), experimental data start to deviate from the fitting below 280 K which indicates that the sample does not obey the Curie-Weiss law.  $\text{Co}_7\text{Zn}_7\text{Mn}_6$  is an itinerant magnetic system and a deviation from the Curie-Weiss law may occur [40].

The isothermal  $M$  vs  $H$  curves recorded at different constant temperatures ( $T = 3$  K, 50 K, 100 K, 125 K, 150 K, 175 K, 190 K, and 300 K), between  $\pm 50$  kOe, are plotted in Fig. 2 (c).  $M$  shows fairly saturating behavior with  $H$  below  $T_c$ . The saturation magnetization ( $M_s$ ) takes maximum value  $9.18 \mu_B/\text{f.u.}$  at 3 K. It is evident [see Fig. 2 (c)] that the sample shows finite coercive field ( $H_C \sim 1$  kOe) only at 3 K, while  $H_C$  is negligible at 100 K data. This is consistent with the previous report that hysteresis loop is only observed below the re-entrant spin glass transition temperature [32].

Interestingly, we observe a virgin loop effect [41, 42] at 3 K, where the virgin line lies outside the hysteresis loop [see Fig. 2 (d)]. Such virgin loop effect often occurs due to the presence of a field induced arrested state. The sample was earlier found to have a spin glass-like state at low temperature, which can be responsible for the virgin

loop effect [43, 44].

Several spin-glass systems were found to show exchange bias (EB) effect [45–48], which is characterized by the horizontal shift (along the  $H$  axis) of the isothermal  $M - H$  curve when cooled under a field ( $H_{cool}$ ) from above the magnetic transition temperature. The values of EB and  $H_C$  can be defined as  $H_{EB} = -(H_{c1} + H_{c2})/2$  and  $H_C = |H_{c1} - H_{c2}|/2$ , where  $H_{c1}$  and  $H_{c2}$  denote the negative and positive fields at which  $M$  turns zero, respectively [49, 50]. Fig. 2 (e) shows the  $M - H$  loops at 3 K both in the ZFC ( $H_{cool} = 0$ ) and FC ( $H_{cool} = 1$  kOe) conditions. Although we recorded the data for  $H = \pm 50$  kOe, an enlarged view in the region  $\pm 4$  kOe are shown for a better clarity. Clearly,  $M - H$  loop shift asymmetrically along the field axis in the direction opposite to  $H_{cool}$ , indicating the presence of finite EB in the system. We recorded the  $M - H$  loops for different values of  $H_{cool}$ , and the variation of  $H_{EB}$  and  $H_C$  with  $H_{cool}$  is shown in Fig. 2 (f).  $H_{EB}$  initially rises sharply with increasing  $H_{cool}$  up to 1 kOe followed by sluggish decrease on higher fields. The maximum value of  $H_{EB}$  is found to be 580 Oe for  $H_{cool} = 1$  kOe at 3 K. The antisite disorder plays an important role towards the observed EB, because it can give rise to varied magnetic interactions depending upon the metal ion and its position in the lattice [51].  $H_C$  follows  $H_{cool}$  variation similar to  $H_{EB}$ .

### C. Electrical Resistivity

We have shown the  $T$  variation of zero-field resistivity [ $\rho_{xx}(T, H = 0)$ ] in the main panel of Fig. 3 (a) for  $\text{Co}_7\text{Zn}_7\text{Mn}_6$  in the range  $5\text{K} \leq T \leq 300\text{K}$ .  $\rho_{xx}$  vs  $T$  data show a typical metallic behavior ( $\frac{d\rho_{xx}}{dT} > 0$ ) in the high- $T$  region. However, below 75 K,  $\rho_{xx}$  starts to rise with decreasing  $T$  giving rise to a resistivity minimum at  $T_{min} = 75$  K. There is a change in slope at  $T_c \sim 200$  K [see the peak in the  $d\rho_{xx}/dT$  curve in the inset (i) of Fig. 3 (a)], which is close to the magnetic transition temperature ( $= 204$  K).

The low- $T$  rise can have multiple origins, such as Kondo effect, WL or EEI [12]. Kondo effect involves

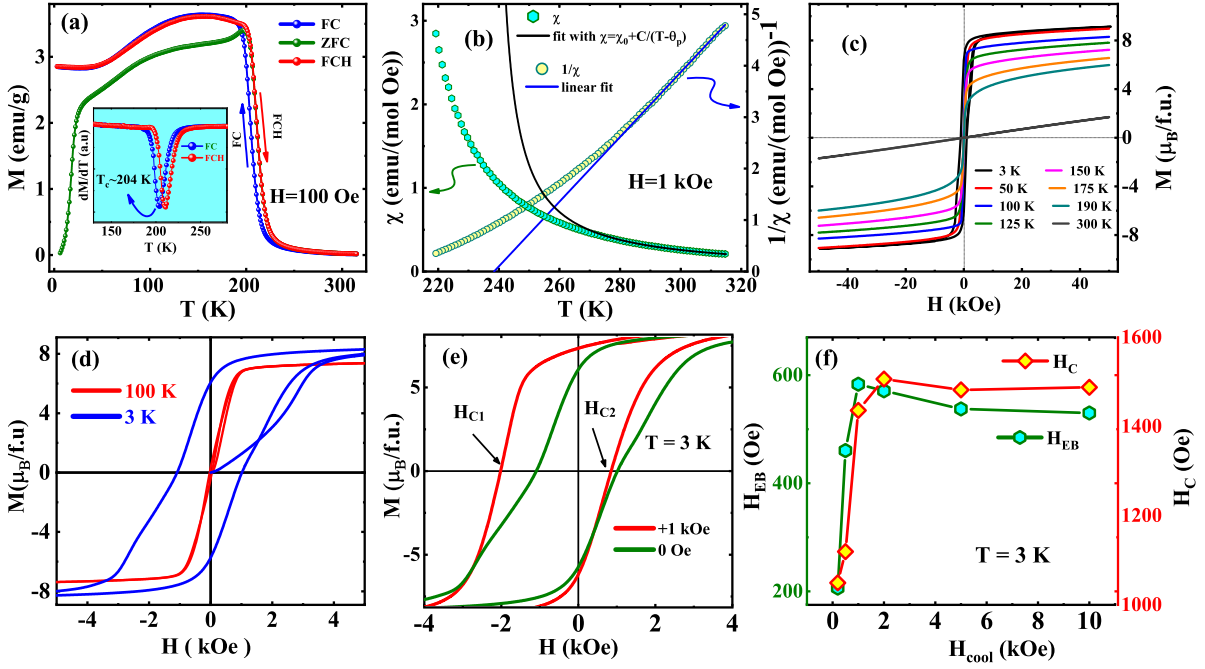


FIG. 2. (a) The magnetisation ( $M$ ) as a function of the temperature ( $T$ ) measured in zero field-cooled-heating (ZFCH), field-cooled (FC) and field-cooled-heating (FCH) protocols under  $H = 100$  Oe. The inset shows the temperature derivative of  $M(T)$ . (b) Susceptibility ( $\chi$ ) versus temperature ( $T$ ) fitted with modified Curie-Weiss law (left axis) and inverse susceptibility ( $\chi^{-1}$ ) versus temperature ( $T$ ) data with linear fitting (right axis), measured at  $H = 1$  kOe. (c) Isothermal magnetization at different temperatures measured between  $\pm 50$  kOe. (d) Enlarge view of the  $M$  vs  $H$  curve at 3 K and 100 K plotted between  $\pm 5$  kOe. (e) Shows isothermal magnetization data measured at 3K after being cooled at zero and +1 k Oe. (f) Shows the variation of exchange bias field ( $H_{EB}$ ) on left axis and coercive field ( $H_C$ ) on right axis as a function of cooling field ( $H_{cool}$ ) at 3K.

$\log(T)$  upturn of  $\rho_{xx}(T)$  at low temperature [52–54], which is absent in our data, and it rules out the Kondo type localization of charge carriers. The contribution from WL to  $\rho_{xx}$  varies as  $T^{p/2}$  ( $p = 3/2, 2$  or  $3$ ) in 3D disordered system [12], and it is very sensitive to  $H$ . In case of  $\text{La}_{1-x}\text{A}_x\text{MnO}_3$  ( $A = \text{Ca, Sr, Ba}$  or  $\text{Pb}$ ), showing resistivity upturn due to WL, the minimum in  $\rho_{xx}$  shifts to lower  $T$  on application of  $H$  and it nearly vanishes for higher applied  $H$  [55, 56].

Altshuler and Aronov have shown that EEI gives rise to increase in  $\rho_{xx}$  with decreasing  $T$  instead of usual metallic behavior [57]. In presence of disorder, the relative change in  $\rho_{xx}$  due to EEI is estimated to be

$$\delta\rho_{xx} = \left[ \frac{\rho_0 - \rho_{xx}(T)}{\rho_0} \right] \propto \frac{\sqrt{T}\tau_e}{(P_F l_e)^2} \quad (1)$$

Here,  $\tau_e$  is the characteristic mean free time,  $P_F$  is Fermi momentum and  $l_e$  is the mean free path between two successive collisions. This expression is valid for  $k_B T \ll \hbar/\tau_e$ , and this inequality is satisfied for  $T < T_{min}$ . The true cause of this upturn below  $T_{min}$  is closely associated with the quantum interference effect in presence of disorder [57–59].

Fig. 3 (b) shows the resistivity minimum of  $\text{Co}_7\text{Zn}_7\text{Mn}_6$  which does not shift with  $H$ . On careful examination of the low- $T$  part of  $\rho_{xx}$ , we find that it follows a  $T^{1/2}$  dependence [see inset of Fig. 3 (a) (ii)] for

both  $H = 0$  and 50 kOe data below about 35 K. This indicates that the EEI plays the dominant role towards the low- $T$  upturn [59, 60]. We observe that  $\rho_{xx}(T, H = 50 \text{ kOe})$  lies below the zero field counterpart due to the small but finite negative magnetoresistance.

Considering all possible contributions to resistivity in our system, we model the  $T$  variation of  $\rho_{xx}$  below  $T_c$  as:

$$\rho_{xx}(T, H) = \rho_{xx0} - \gamma_{EEI} T^{1/2} + \beta_{e-m} T^2 + \alpha_{e-p} (T/\theta_D)^5 \int_0^{\theta_D/T} \frac{x^5 dx}{(e^x - 1)(1 - e^{-x})} \quad (2)$$

In eqn. 2,  $\rho_{xx0}$  is a temperature independent term, while the second and the third terms respectively represent the electron-electron (e-e) interaction and electron-magnon (e-m) scattering contribution. The last term represents the electron-phonon (e-p) scattering contribution according to Bloch-Grüneisen model ( $\theta_D$  is the Debye temperature) [61]. The continuous lines in Fig. 3 (b) indicate the fitting to the data by eqn. 2 for both  $H = 0$  and 50 kOe curves below 100 K. The fitting parameters are provided in table I. We choose  $\theta_D$  to be 320 K for both the values of  $H$ . The coefficient of electron-magnon scattering term ( $\beta_{e-m}$ ) decreases under  $H$ , because an applied field reduces the spin-disorder scattering.

We also studied the isothermal  $H$  variation of  $\rho_{xx}$  at different  $T$ . The field variation of magnetoresistance

$H$ (kOe)	$\rho_{xx0}$ ( $\mu\Omega$ cm)	$\gamma_{EEI}$ ( $\mu\Omega$ cm $K^{-1/2}$ )	$\beta_{e-m}$ ( $\mu\Omega$ cm $K^{-2}$ )	$\alpha_{e-p}$ ( $\mu\Omega$ cm)
0	189.54(2)	0.36(3)	$11.7(7) \times 10^{-5}$	0.83(3)
50	188.81(3)	0.34(3)	$10.2(3) \times 10^{-5}$	0.82(8)

TABLE I. The fitting parameters obtained by fitting the resistivity data using eqn. 2

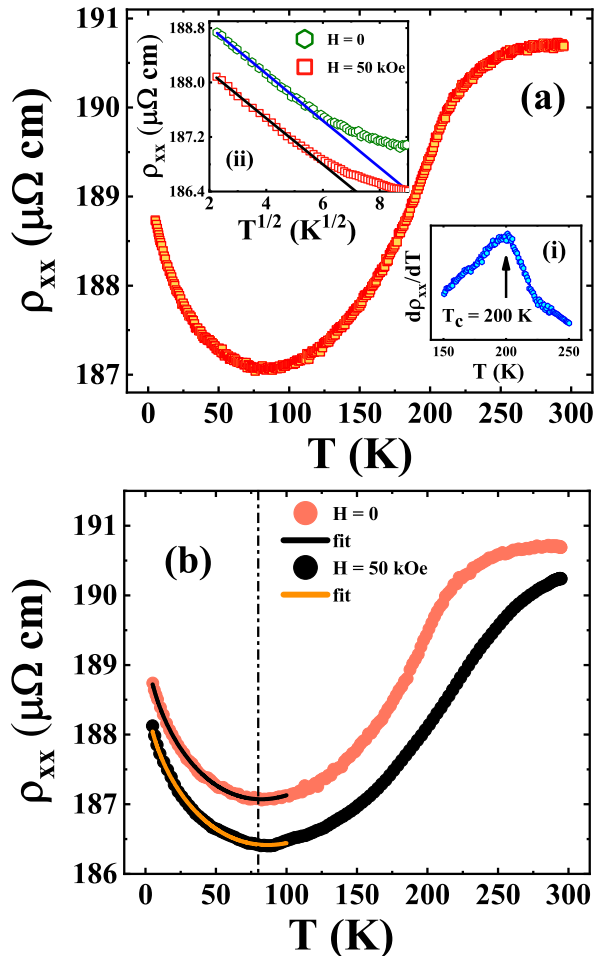


FIG. 3. (a) shows the  $T$  variation of resistivity ( $\rho_{xx}$ ). The inset a(i) shows the  $\frac{d\rho_{xx}}{dT}$  vs  $T$  curve and a(ii) shows  $\rho_{xx}$  vs  $T^{1/2}$  plot below 50 K, along with a linear fit to the data. (b) shows  $\rho_{xx}$  vs  $T$  data at  $H=0, 50$  kOe fitted with eqn. 2

(MR) [ $= (\rho_{xx}(H) - \rho_{xx}(0))/(\rho_{xx}(0))$ ] is shown in Fig. 4 (a). At 300 K, MR is found to obey an  $H^2$  dependence [see inset of Fig. 4 (b)], while MR shows a  $H^{2/3}$  variation around  $T_c$  [see main panel of 4 (b)]. Well below  $T_c$  (150, 120 K), a linear variation of MR with  $H$  is found [see Fig. 4 (c)]. It is generally believed that for a  $3d$  transition metal based intermetallic alloy showing FM-like order, the magnetic contribution to the resistivity arises due to the scattering of the delocalized  $s$  electrons with the partially localized  $3d$  electrons. Under the ap-

plication of  $H$ , the spin dependent scattering diminishes leading to negative MR.

Although the value of MR is quite small, its field variation in different  $T$  range is quite interesting. There are several theoretical works addressing the  $H$  dependence of MR in the transition metal based itinerant magnets [62, 63], and the theory predicts an  $H^{2/3}$  variation around  $T_c$  [63], which is also the case for our present sample. A linear  $H$  variation of MR is predicted in the  $s-d$  scattering model, which is clearly observed here. The high temperature (well above  $T_c$ )  $H^2$  variation of MR in the  $s-d$  model is also evident in our 300 K data. It is clear that the observed small negative MR in the present compound arises due to the suppression of  $s-d$  scattering by the applied field, and  $\text{Co}_7\text{Zn}_7\text{Mn}_6$  is turned out to be classic example where the prevailing theory of MR works well at least up to 50 kOe.

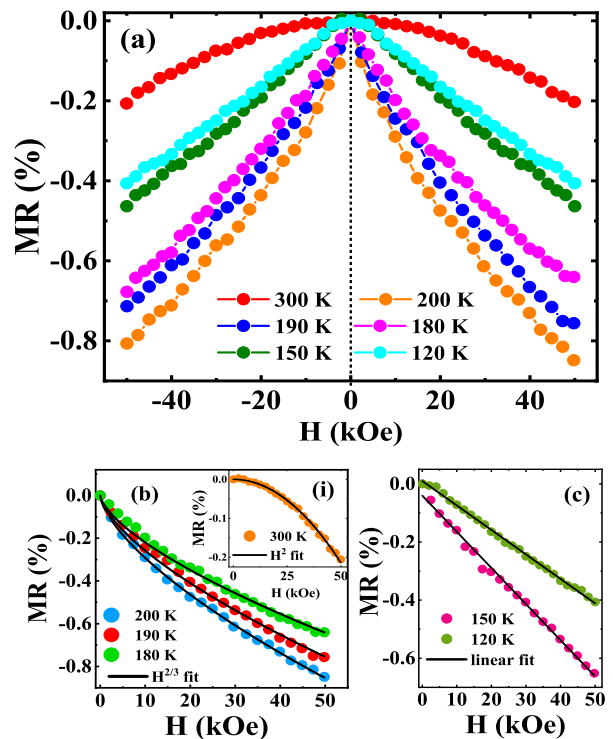


FIG. 4. (a) shows isothermal field dependent MR. (b) main panel shows  $H^{2/3}$  dependence of MR vs  $H$  near the transition temperature, inset shows the  $H^2$  dependence of MR vs  $H$  at 300 K. (c) shows the linear field dependence of MR well below the transition temperature.

#### D. Hall measurements

The major outcome of the present work is based on the Hall effect study of  $\text{Co}_7\text{Zn}_7\text{Mn}_6$ . The Hall resistivity ( $\rho_{xy}$ ) data as a function of  $H$  at various  $T$  are shown in Fig. 5(a). Here, the current is allowed to flow along the  $x$  axis, while the Hall voltage was measured along the  $y$

direction with the magnetic field along the  $z$  axis. We measured  $\rho_{xy}$  for both positive and negative values of  $H$ , and the final  $\rho_{xy}$  versus  $H$  plot was drawn using the formula  $\rho_{xy}(H) = \frac{1}{2}[\rho_{xy}(+H) - \rho_{xy}(-H)]$ . This helps us to eliminate any MR contribution in the data. The  $\rho_{xy}(H)$  is found to be highly nonlinear below about 200 K indicating the presence of AHE. There is a sharp increase in the low field region ( $H=0 \sim 5$  kOe), and the data tend to saturate at higher fields with small positive slope. This sluggish increase in  $\rho_{xy}$  at higher  $H$  is due to the contribution from ordinary Hall effect (OHE).  $\rho_{xy}(H)$  mimics the  $M$  versus  $H$  data indicating the influence of  $M$  towards the Hall voltage. Notably,  $\rho_{xy}(H)$  is linear at 300 K (well above  $T_c$ ), because AHE vanishes in the paramagnetic state.

Typically in a magnetic material with magnetization  $M$ ,  $\rho_{xy}$  can be expressed as (in cgs unit)

$$\rho_{xy} = \rho_{xy}^{OHE} + \rho_{xy}^{AHE} = R_0 H + 4\pi R_S M \quad (3)$$

where,  $\rho_{xy}^{OHE}$  and  $\rho_{xy}^{AHE}$  are the ordinary and anomalous Hall resistivities with coefficients  $R_0$  and  $R_S$  respectively. By linear fitting the high field region ( $H \geq 30$  kOe) of the  $\rho_{xy}$  vs  $H$  curve [Fig. 5(b)], we obtain  $\rho_{xy}^{AHE}$  and  $R_0$  from the  $y$ -intercept and the slope, respectively. The  $\rho_{xy}^{AHE}$  is found to decrease monotonously with increasing temperature [see Fig. 5(c)]. The anomalous Hall conductivity ( $\sigma_{xy}^{AHE}$ ) is calculated using the formula  $\sigma_{xy}^{AHE} = -\rho_{xy}^{AHE} / [(\rho_{xy}^{AHE})^2 + (\rho_{xx})^2]$  and its temperature dependence is shown in Fig. 5(d).

$M_s$  vs  $T$  curve [see inset of Fig. 5(d)] is found to obey the well-known spin-wave (SW) equation [64, 65]

$$M_s(T) = M_s(0)(1 - AT^{3/2} - BT^{5/2}) \quad (4)$$

Here  $M_s(0)$  is the value at 0 K. The fitted values of the parameters  $A$  and  $B$  are found to be  $2.928 \times 10^{-5} \text{ K}^{-3/2}$  and  $5.531 \times 10^{-7} \text{ K}^{-5/2}$  respectively. Interestingly,  $\sigma_{xy}^{AHE}$  follows a similar equation that of eqn. 4 [i.e.  $\sigma_{xy}^{AHE} \propto (1 - AT^{3/2} - BT^{5/2})$ ] down to 5 K without any visible anomaly below  $T_{min}$  and the corresponding fitted parameters  $A$  and  $B$  are  $8.25 \times 10^{-5} \text{ K}^{-3/2}$  and  $5.292 \times 10^{-7} \text{ K}^{-5/2}$  respectively. The absence of any anomaly below  $T_{min}$  indicates that both  $\sigma_{xy}^{AHE}$  and  $\rho_{xy}^{AHE}$  remain unaffected by the e-e localization effect present in  $\rho_{xx}$  within the accuracy of our measurements. To check the result, we measured Hall voltage using two different instruments (from Quantum Design, USA and Cryogenic Ltd, UK). However, data from both the measurements are identical providing no signature of EEI to AHE. This finding provides an experimental evidence to the theoretical prediction [19, 20] that the correction to  $\sigma_{xy}^{AHE}$  is identically zero even though there is a finite low- $T$  upturn in the  $\rho_{xx}(T)$  data due to EEI.

Fig. 5(e) shows the temperature variation of  $R_0$  and  $R_S$  calculated using the formula  $R_S = \rho_{xy}^{AHE} / (4\pi M_S)$ . It is clearly seen that the localization effect is present in  $R_0$  at low temperature but not in  $R_S$ .  $R_S$  is found to be two

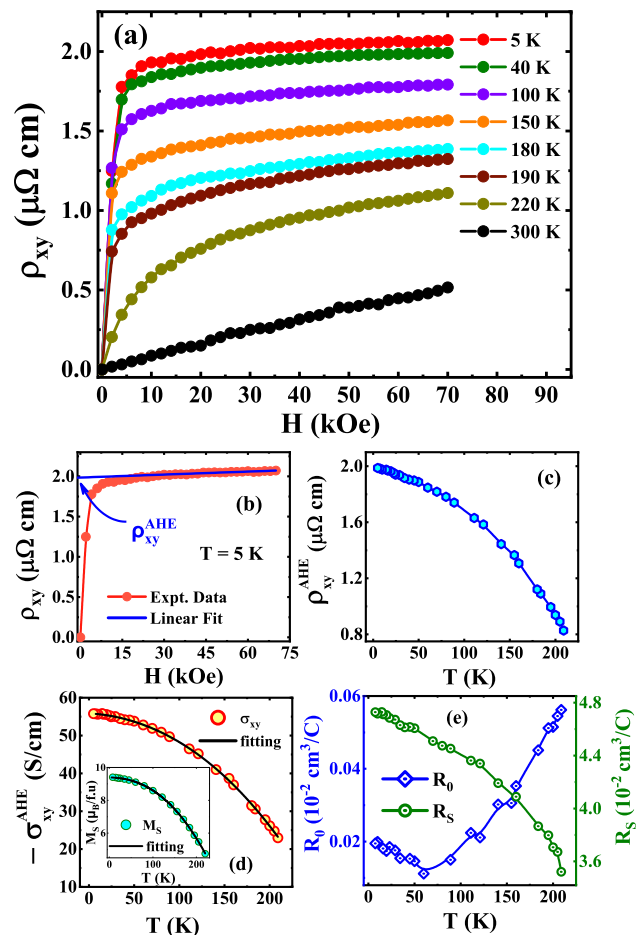


FIG. 5. (a) Hall resistivity ( $\rho_{xy}$ ) vs  $H$  at different constant  $T$ . (b) shows  $\rho_{xy}$  vs  $H$  at  $T = 5$  K with a linear fit to the high field data. ( $\rho_{xy}$ ) vs  $H$ ,  $\rho_{xy}^{AHE} / \rho_{xx}$  vs  $\rho_{xx}$  plot with linear fit. (c)  $T$  variation of  $\rho_{xy}^{AHE}$ . (d)  $\sigma_{xy}^{AHE}$  vs  $T$  fitted with eqn. 4 and the inset shows the saturation magnetization ( $M_s$ ) as a function of  $T$  and fitted with eqn. 4. (e)  $T$  variation of ordinary Hall coefficient ( $R_0$ ) and anomalous Hall coefficient ( $R_S$ ).

order of magnitude greater than the  $R_0$ , which indicates the dominance of anomalous Hall resistivity. The coefficient  $R_0$  is found to be positive, which indicates holes as majority charge carriers. The carrier concentration ( $n_h$ ) is calculated using  $n_h = 1/(R_0 e)$ , and it is found to be  $3.2 \times 10^{22} \text{ cm}^{-3}$  at 5 K.

#### IV. DISCUSSION

The most important observation from the present study is associated with the electronic transport study of  $\text{Co}_7\text{Zn}_7\text{Mn}_6$ . We find a robust upturn in the longitudinal resistivity versus temperature data below about 75 K, which remains almost unaffected even under 50 kOe of field. Such low temperature upturn in otherwise metallic alloy is generally attributed to localization of charge

carriers. Our careful investigation of zero field and with field  $\rho_{xx}(T)$  data show that at low temperature  $\rho_{xx}(T)$  follow  $T^{1/2}$  dependence [see inset of Fig. 3 (a)], which confirms that the electron-electron interaction is primarily responsible for this low- $T$  upturn [12]. Evidently, this EEI mechanism is insensitive to the magnetic field (at least for  $H \leq 50$  kOe).

The signature of EEI is also seen in the regular Hall coefficient,  $R_0$ . It shows an upturn below about 70 K, which is similar to the upturn in  $\rho_{xx}(T)$ . A rise in  $R_0$  also indicates a decrease in free charge carriers as  $R_0 = 1/(ne)$ , where  $n$  is the carrier concentration and  $e$  is the electronic charge. Interestingly, the localization effect observed in  $\rho_{xx}(T)$  and  $R_0$  at low temperature is completely absent in all components of AHE, *i.e.*, in  $\rho_{xy}^{AHE}(T)$ ,  $R_s(T)$  and even in  $\sigma_{xy}^{AHE}(T)$ . As evident from Fig. 5(d),  $\sigma_{xy}^{AHE}(T)$  varies monotonously and it obeys the SW equation (eqn. 4). The fit with SW law does not show any deviation at low temperature, particularly below 75 K, where EEI localization in  $\rho_{xx}$  and  $R_0$  is evident. This result supports the previous theoretical prediction that EEI correction to AHE identically vanishes for both skew scattering and side-jump mechanisms [19, 20]. It is to be noted that the change in the carrier concentration due to localization, as obtained from ordinary Hall coefficient, is  $5.57 \times 10^{22}$  (at 60 K) to  $3.2 \times 10^{22}$  (at 5 K). Such change may not affect the electronic energy band structure required for change in anomalous Hall coefficient.

Recently Yang *et al.* showed the presence of EEI contribution towards the AHE in the semiconducting  $\text{HgCr}_2\text{Se}_4$  single crystal with a  $T^{1/2}$  dependence of  $\sigma_{xy}^{AHE}(T)$  at sub Kelvin temperature [25]. The compound shows low- $T$  electron localization due to EEI with  $\rho_{xx}(T) \propto T^{1/2}$ . The theories that rule out the contribution of EEI to AHE [19, 20] assume (i) the sample to have the mirror symmetry in its crystal structure, and (ii) take care only the extrinsic mechanisms (side jump and skew scattering) ignoring the Berry phase induced intrinsic mechanism. Yang *et al.* argued that although  $\text{HgCr}_2\text{Se}_4$  possess overall mirror symmetry, it may be broken locally at the site of the disorder. In addition, intrinsic contribution of Hall effect may also play a role towards the observed localization effect in

$\sigma_{xy}^{AHE}(T)$ . The effect of EEI in  $\sigma_{xy}^{AHE}(T)$  is further substantiated by a recent theoretical work [26], which proposed that  $\sigma_{xy}^{AHE}(T)$  should follow  $T^{1/2}/\ln(T_0/T)$  (for 3D systems) type  $T$  dependence due to EEI effect at low- $T$ . This theory takes into account the contribution from Cooper channel for the purely repulsive interaction in a non-superconducting metal, which was overlooked in the previous studies.  $\text{HgCr}_2\text{Se}_4$  system has relatively lower carrier density ( $\sim 10^{15}-10^{18}$   $\text{cm}^{-3}$ ) and  $\rho_{xx} \sim 10^{-2}$   $\Omega$  cm, whereas in  $\text{Co}_7\text{Zn}_7\text{Mn}_6$ , the carrier density is found to  $10^{22}$   $\text{cm}^{-3}$  and  $\rho_{xx} \sim 2 \times 10^{-5}$   $\Omega$  cm. The low carrier density in  $\text{HgCr}_2\text{Se}_4$  may have an influence on the observed correction in  $\sigma_{xy}^{AHE}(T)$ . Notably, the effect of carrier localization in AHE is also absent in  $\text{Co}_2\text{FeSi}$  thin films [13] and  $\text{Zr}_{1-x}\text{V}_x\text{Co}_{1.6}\text{Sn}$  semimetal [27], which are otherwise metallic with large carrier density.

Though there is a lattice anomaly at around 40 K, it is not reflected in our Hall conductivity data. The change in  $a$  is only 0.03%, which possibly too weak to provide any detectable signature in our Hall data.

In conclusion, we fail to observe the effect of correlation induced electron localization in the anomalous Hall effect in the chiral compound  $\text{Co}_7\text{Zn}_7\text{Mn}_6$ . Although this result is consistent with the theoretical models proposed by the group of P. Wölfle [19, 20], it is in sharp contrast with recent experimental and theoretical works [25, 26]. The most of the theories proposed so far consider the presence of mirror symmetry in the lattice and primarily concentrated on extrinsic mechanisms. Therefore, it is important to address the issue with theoretical models where the system has broken mirror symmetry (such as the present  $\text{Co}_7\text{Zn}_7\text{Mn}_6$ ) and with the inclusion of intrinsic contribution towards AHE.

## ACKNOWLEDGMENTS

PC wishes to thank DST-INSPIRE program for the research assistance. The UGC DAE-CSR Kolkata center, where the low-temperature magneto-resistance measurements were performed, is duly acknowledged. We thank Prof. Chandan Mazumdar, SINP, Kolkata for Hall measurements.

- 
- [1] E. H. Hall, On a New Action of the Magnet on Electric Currents, *Am. J. Math.* **2**, 287 (1879).
  - [2] E. H. Hall, On the new action of magnetism on a permanent electric current, *Philos. Mag.* **12**, 301 (1880).
  - [3] E. H. Hall, On the "Rotational Coefficient" in nickel and cobalt, *Philos. Mag.* **12**, 157-172 (1881).
  - [4] C. M. Hurd, The Hall effect in metals and alloys, (Plenum Press, New York (1972).
  - [5] Naoto Nagaosa, Jairo Sinova, Shigeki Onoda, A. H. MacDonald, and N. P. Ong, Anomalous Hall effect, *Rev. Mod. Phys.* **82**, 1539 (2010).
  - [6] Robert Karplus and J. M. Luttinger, Hall Effect in Ferromagnetics, *Phys. Rev.* **95**, 1154 (1954).
  - [7] Di Xiao, Ming-Che Chang, and Qian Niu, Berry phase effects on electronic properties, *Rev. Mod. Phys.* **82**, 1956 (2010).
  - [8] J. Smit, The spontaneous hall effect in ferromagnetics I, *Physica (Amsterdam)* **21**, 877 (1955).
  - [9] J. Smit, The spontaneous hall effect in ferromagnetics II, *Physica (Amsterdam)* **24**, 39 (1958).
  - [10] L. Berger, Side-Jump Mechanism for the Hall Effect of Ferromagnets, *Phys. Rev. B* **2**, 4559 (1970).

- [11] Gerd Bergmann, Weak localization in thin films: a time-of-flight experiment with conduction electrons, *Phys. Rep.* **107**, 1 (1984).
- [12] Patrick A. Lee and T. V. Ramakrishnan, Disordered electronic systems, *Rev. Mod. Phys.* **57**, 287 (1985).
- [13] Binoy Krishna Hazra, S. N. Kaul, S. Srinath, M. Manivel Raja, R. Rawat, and Archana Lakhani, Evidence for the absence of electron-electron Coulomb interaction quantum correction to the anomalous Hall effect in  $\text{Co}_2\text{FeSi}$  Heusler-alloy thin films, *Phys. Rev. B* **96**, 184434 (2017).
- [14] Lin Wu, Kai Zhu, Di Yue, Yuan Tian, and Xiaofeng Jin, Anomalous Hall effect in localization regime, *Phys. Rev. B* **93**, 214418 (2016).
- [15] Hendrik Meier, Maxim Yu. Kharitonov, and Konstantin B. Efetov, Anomalous Hall effect in granular ferromagnetic metals and effects of weak localization, *Phys. Rev. B* **80**, 045122 (2009).
- [16] P. Mitra, N. Kumar, and N. Samarth, Localization and the anomalous Hall effect in a dirty metallic ferromagnet, *Phys. Rev. B* **82**, 035205 (2010).
- [17] Gerd Bergmann, B. L. Altshuler, and A. G. Aronov, Electron-Electron Interactions in Disordered Systems, edited by A. L. Efros and M. Pollak, (North-Holland, Amsterdam, 1985).
- [18] V. K. Dugaev, A. Crépieux, and P. Bruno, Localization corrections to the anomalous Hall effect in a ferromagnet, *Phys. Rev. B* **64**, 104411 (2001).
- [19] K. A. Muttalib and P. Wölfle, Disorder and temperature dependence of the anomalous Hall effect in thin ferromagnetic films: Microscopic model, *Phys. Rev. B* **76**, 214415 (2007).
- [20] Annette Langenfeld and Peter Wölfle, Absence of quantum corrections to the anomalous Hall conductivity, *Phys. Rev. Lett.* **67**, 739 (1991).
- [21] P. Mitra, R. Misra, A. F. Hebard, K. A. Muttalib, and P. Wölfle, Weak-Localization Correction to the Anomalous Hall Effect in Polycrystalline Fe Films, *Phys. Rev. Lett.* **99**, 046804 (2007).
- [22] Z. B. Guo, W. B. Mi, Q. Zhang, B. Zhang, R. O. Aboljadayel, and X. X. Zhang, Anomalous Hall effect in polycrystalline Ni films, *Solid State Commun.* **152**, 220 (2012).
- [23] Y. M. Lu, J. W. Cai, Zaibing Guo, and X. X. Zhang, Unconventional scaling of the anomalous Hall effect accompanying electron localization correction in the dirty regime, *Phys. Rev. B* **87**, 094405 (2013).
- [24] Yan Zhang, Wenbo Mi, Xiaocha Wang, and Zaibing Guo, Scaling of anomalous Hall effect in amorphous  $\text{CoFeB}$  films with accompanying quantum correction, *Solid State Commun.* **5**, 215-216 (2015).
- [25] Shuai Yang, Zhilin Li, Chaojing Lin, Changjiang Yi, Youguo Shi, Dimitrie Culcer, and Yongqing Li, Unconventional Temperature Dependence of the Anomalous Hall Effect in  $\text{HgCr}_2\text{Se}_4$ , *Phys. Rev. Lett.* **123**, 096601 (2019).
- [26] Songci Li and Alex Levchenko, Temperature Dependence of the Anomalous Hall Effect from Electron Interactions, *Phys. Rev. Lett.* **124**, 156802 (2020).
- [27] Guangqiang Wang, Zhanghao Sun, Xinyu Si, and Shuang Jia, Anomalous Hall effect in ferromagnetic Weyl semimetal candidate  $\text{Zr}_{1-x}\text{V}_x\text{Co}_{1.6}\text{Sn}$ , *Chinese Phys. B* **29**, 077503 (2020).
- [28] K. Karube, J. S. White, V. Ukleev, C. D. Dewhurst, R. Cubitt, A. Kikkawa, Y. Tokunaga, H. M. Rønnow, Y. Tokura, and Y. Taguchi, Metastable skyrmion lattices governed by magnetic disorder and anisotropy in  $\beta$ -Mn-type chiral magnets, *Phys. Rev. B* **102**, 064408 (2020).
- [29] K. Karube, J. S. White, N. Reynolds, J. L. Gavilano, H. Oike, A. Kikkawa, F. Kagawa, Y. Tokunaga, H. M. Rønnow, Y. Tokura, *et al.*, Robust metastable skyrmions and their triangular-square lattice structural transition in a high-temperature chiral magnet, *Nat. Mater.* **15**, 1237-1242 (2016).
- [30] Y. Tokunaga, X. Z. Yu, J. S. White, H. M. Rønnow, D. Morikawa, Y. Taguchi, and Y. Tokura, A new class of chiral materials hosting magnetic skyrmions beyond room temperature, *Nat. Commun.* **6**, 7638 (2015).
- [31] T.Hori, H.Shiraish, and Y.Ishii, Magnetic properties of  $\beta$ -MnCoZn alloys, *J. Magn. Magn. Mater.* **310**, 1820 (2007).
- [32] Joshua D. Bocarsly, Colin Heikes, Craig M. Brown, Stephen D. Wilson, and Ram Seshadri, Deciphering structural and magnetic disorder in the chiral skyrmion host materials  $\text{Co}_x\text{Zn}_y\text{Mn}_z$  ( $x + y + z = 20$ ), *Phys. Rev. Materials* **3**, 014402 (2019).
- [33] T. Nakajima, K. Karube, Y. Ishikawa, M. Yone-mura, N. Reynolds, J. S. White, H. M. Rønnow, A. Kikkawa, Y. Tokunaga, Y. Taguchi, *et al.*, Correlation between site occupancies and spin-glass transition in skyrmion host  $\text{Co}_{10-x/2}\text{Zn}_{10-x/2}\text{Mn}_x$ , *Phys. Rev. B* **100**, 064407 (2019).
- [34] Kosuke Karube, Jonathan S. White, Daisuke Morikawa, Charles D. Dewhurst, Robert Cubitt, Akiko Kikkawa, Xiuzhen Yu, Yusuke Tokunaga, Taka-hisa Arima, Henrik M. Rønnow, *et al.*, Disordered skyrmion phase stabilized by magnetic frustration in a chiral magnet, *Sci. Adv.* **4**, eaar7043 (2018).
- [35] Daisuke Morikawa, Xiuzhen Yu, Kosuke Karube, Yusuke Tokunaga, Yasujiro Taguchi, Taka-hisa Arima, and Yoshinori Tokura, Deformation of Topologically-Protected Supercooled Skyrmions in a Thin Plate of Chiral Magnet  $\text{Co}_8\text{Zn}_8\text{Mn}_4$ , *Nano Lett.* **17**, 1637-1641 (2017).
- [36] Fangyi Qi, Yalei Huang, Xinyu Yao, Wenlai Lu, and Guixin Cao, Anomalous electrical transport and magnetic skyrmions in Mn-tuned  $\text{Co}_9\text{Zn}_9\text{Mn}_2$  single crystals, *Phys. Rev. B* **107**, 115103 (2023).
- [37] Hai Zenga, Xuanwei Zhaoa, Guang Yua, Xiaohua Luoa, Shengcan Maa, Changcai Chena, Zhaojun Mog, Yungang Zhange, Yisheng Chaie, Jun Shen, *et al.*, Magnetic and transport properties of chiral magnet  $\text{Co}_7\text{Zn}_8\text{Mn}_5$ , *J. Magn. Magn. Mater.* **560**, 169631 (2022).
- [38] L. Lutterotti, M. Bortolotti, G. Ischia, I. Lonardelli, and H.-R. Wenk, Rietveld texture analysis from diffraction images, **26**, 126 (2007).
- [39] K. Karube, K. Shibata, J. S. White, T. Koretsune, X. Z. Yu, Y. Tokunaga, H. M. Rønnow, R. Arita, T. Arima, Y. Tokura, *et al.*, Controlling the helicity of magnetic skyrmions in a  $\beta$ -Mn-type high-temperature chiral magnet, *Phys. Rev. B* **98**, 155120 (2018).
- [40] F. R. de Boer, C. J. Schinkel, J. Biesterbos, and S. Proost, Exchange-Enhanced Paramagnetism and Weak Ferromagnetism in the  $\text{Ni}_3\text{Al}$  and  $\text{Ni}_3\text{Ga}$  Phases; Giant Moment Inducement in Fe-Doped  $\text{Ni}_3\text{Ga}$ , *J. Appl. Phys.* **40**, 1049-1055 (1969).

- [41] M. K. Chattopadhyay and S. B. Roy, Meta-magnetic transition and the anomalous virgin magnetization curve in  $\text{Ce}(\text{Fe}_{0.96}\text{Ru}_{0.04})_2$ , *J. Phys.: Condens. Matter* **20**, 025209 (2008).
- [42] M. A. Manekar, S. Chaudhary, M. K. Chattopadhyay, K. J. Singh, S. B. Roy, and P. Chaddah, First-order transition from antiferromagnetism to ferromagnetism in  $\text{Ce}(\text{Fe}_{0.96}\text{Al}_{0.04})$ , *Phys. Rev. B* **64**, 104416 (2001).
- [43] C. A. Cardoso, F. M. Araujo-Moreira, V. P. S. Awana, E. Takayama-Muromachi, O. F. de Lima, H. Yamauchi, and M. Karppinen, Spin glass behavior in  $\text{RuSr}_2\text{Gd}_{1.5}\text{Ce}_{0.5}\text{Cu}_2\text{O}_{10-\delta}$ , *Phys. Rev. B* **67**, 020407(R) (2003).
- [44] P. Neenu Lekshmi, G. R. Raji, M. Vasundhara, Manoj Raama Varma, S. Savitha Pillai, and M. Valant, Re-entrant spin glass behaviour and magneto-dielectric effect in insulating  $\text{Sm}_2\text{NiMnO}_6$  double perovskite, *J. Mater. Chem. C* **1**, 6565 (2013).
- [45] S. Giri, M. Patra, and S. Majumdar, Exchange bias effect in alloys and compounds, *J. Phys.: Condens. Matter* **23**, 073201 (2011).
- [46] Johannes Kroder, Kaustuv Manna, Dominik Kriegner, A. S. Sukhanov, Enke Liu, Horst Borrmann, Andreas Hoser, Johannes Gooth, Walter Schnelle, Dmytro S. Inosov, *et al.*, Spin glass behavior in the disordered half-Heusler compound  $\text{IrMnGa}$ , *Phys. Rev. B* **99**, 174410 (2019).
- [47] Rahul Kumar, Premakumar Yanda, and A. Sundaresan, Cluster-glass behavior in the two-dimensional triangular lattice Ising-spin compound  $\text{Li}_2\text{Mn}_3\text{O}_7$ , *Phys. Rev. B* **103**, 214427 (2021).
- [48] R. C. Sahoo, Y. Takeuchi, A. Ohtomo, and Z. Hossain, Exchange bias and spin glass states driven by antisite disorder in the double perovskite compound  $\text{LaSrCoFeO}_6$ , *Phys. Rev. B* **100**, 214436 (2021).
- [49] R. L. Stamps, Mechanisms for exchange bias, *J. Phys. D* **33**, R247 (2000).
- [50] Jyoti Sharma and K. G. Suresh, Observation of giant exchange bias in bulk  $\text{Mn}_{50}\text{Ni}_{42}\text{Sn}_8$  Heusler alloy, *Appl. Phys. Lett.* **106**, 072405 (2015).
- [51] A. K. Nayak, M. Nicklas, S. Chadov, C. Shekhar, Y. Skourski, J. Winterlik, and C. Felser, Large Zero-Field Cooled Exchange-Bias in Bulk  $\text{Mn}_2\text{PtGa}$ , *Phys. Rev. Lett.* **110**, 127204 (2013).
- [52] S. N. Kaul, W. Kettler, and M. Rosenberg, Electrical resistivity of amorphous  $\text{Fe}_{82}\text{B}_{18-x}\text{Ge}_x$  alloys: Coherent electron-magnon scattering contribution, *Phys. Rev. B* **35**, 7153 (1987).
- [53] P. D. Babu, S. N. Kaul, L. Fernández Barquín, J. C. Gomez Sal, W. H. Kettler, and M. Rosenberg, Electron-electron interaction, quantum interference and spin fluctuation effects in the resistivity of Fe-rich Fe-Zr metallic glasses, *Int. J. Mod. Phys. B* **13**, 141–159 (1999).
- [54] M. Vasundhara, V. Srinivas, and V. V. Rao, Electronic transport in Heusler-type  $\text{Fe}_2\text{VAl}_{1-x}\text{Mn}_x$  alloys ( $M = \text{B}, \text{In}, \text{Si}$ ), *Phys. Rev. B* **77**, 224415 (2008).
- [55] E. Rozenberg, M. Auslender, I. Felner, and G. Gorodetsky, Low-temperature resistivity minimum in ceramic manganites, *J. Appl. Phys.* **88**, 2578–2582 (2000).
- [56] Yan Xu, Jincang Zhang, Guixin Cao, Chao Jing, and Shixun Cao, Low-temperature resistivity minimum and weak spin disorder of polycrystalline  $\text{La}_{2/3}\text{Ca}_{1/3}\text{MnO}_3$  in a magnetic field, *Phys. Rev. B* **73**, 224410 (2006).
- [57] B. L. Al'fshuler and A. G. Aronov, Contribution to the theory of disordered metals in strongly doped semiconductors, *Sov. Phys. JEPT* **50**, 5 (1979).
- [58] A. Aronov, Fourteen years of quantum interference in disordered metals, *Phys. Scr.* **28**, 1993 (1993).
- [59] Wei Niu, Ming Gao, Xuefeng Wang, Fengqi Song, Jun Du, Xinran Wang, Yongbing Xu, and Rong Zhang, Evidence of weak localization in quantum interference effects observed in epitaxial  $\text{La}_{0.7}\text{Sr}_{0.3}\text{MnO}_3$  ultrathin films, *Sci. Rep.* **6**, 26081 (2016).
- [60] M. Ziese, Searching for quantum interference effects in  $\text{La}_{0.7}\text{Sr}_{0.3}\text{MnO}_3$  films on  $\text{SrTiO}_3$ , *Phys. Rev. B* **68**, 132411 (2003).
- [61] Dirk Bombor, Christian G. F. Blum, Oleg Volkonskiy, Steven Rodan, Sabine Wurmehl, Christian Hess, and Bernd Büchner, Half-Metallic Ferromagnetism with Unexpectedly Small Spin Splitting in the Heusler Compound  $\text{Co}_2\text{FeSi}$ , *Phys. Rev. Lett.* **110**, 066601 (2013).
- [62] B. Raquet, M. Viret, E. Sondergard, O. Cespedes, and R. Mamy, Electron-magnon scattering and magnetic resistivity in  $3d$  ferromagnets, *Phys. Rev. B* **66**, 024433 (2002).
- [63] H. Yamada and S. Takada, Magnetoresistance of Antiferromagnetic Metals Due to s-d Interaction, *J. Phys. Soc. Jpn.* **34**, 51 (1973).
- [64] S. N. Kaul, Low-temperature magnetization and spin-wave excitations in amorphous Ni-rich transition-metal—metalloid alloys, *Phys. Rev. B* **27**, 5761 (1983).
- [65] S. N. Kaul and P. D. Babu, Detailed magnetization study of quenched random ferromagnets. I. Low-lying magnetic excitations, *Phys. Rev. B* **50**, 9308 (1994).